Journal of Biomedical Optics

SPIEDigitalLibrary.org/jbo

Methylene blue microbubbles as a model dual-modality contrast agent for ultrasound and activatable photoacoustic imaging

Mansik Jeon
Wentao Song
Elizabeth Huynh
Jungho Kim
Jeesu Kim
Brandon L. Helfield
Ben Y. C. Leung
David E. Goertz
Gang Zheng
Jungtaek Oh
Jonathan F. Lovell
Chulhong Kim

SPIE

Methylene blue microbubbles as a model dual-modality contrast agent for ultrasound and activatable photoacoustic imaging

Mansik Jeon,[a,*,†] Wentao Song,[b,†] Elizabeth Huynh,[c] Jungho Kim,[d] Jeesu Kim,[a] Brandon L. Helfield,[c] Ben Y. C. Leung,[e] David E. Goertz,[c,e] Gang Zheng,[c] Jungtaek Oh,[d] Jonathan F. Lovell,[b] and Chulhong Kim[a]
[a]Pohang University of Science and Technology, Departments of Electrical Engineering and Creative IT Engineering, 77 Cheongam-Ro, Nam-Gu, Pohang, Gyeongbuk, 790-784, Republic of Korea
[b]State University of New York, The University at Buffalo, Department of Biomedical Engineering, Buffalo, New York 14260
[c]University of Toronto, Department of Medical Biophysics, Toronto M5S 1A1, Canada
[d]Samsung Medison, Seoul, 135-851, Republic of Korea
[e]Sunnybrook Health Sciences Center, Toronto M5S 1A1, Canada

Abstract. Ultrasound and photoacoustic imaging are highly complementary modalities since both use ultrasonic detection for operation. Increasingly, photoacoustic and ultrasound have been integrated in terms of hardware instrumentation. To generate a broadly accessible dual-modality contrast agent, we generated microbubbles (a standard ultrasound contrast agent) in a solution of methylene blue (a standard photoacoustic dye). This MB^2 solution was formed effectively and was optimized as a dual-modality contrast solution. As microbubble concentration increased (with methylene blue concentration constant), photoacoustic signal was attenuated in the MB^2 solution. When methylene blue concentration increased (with microbubble concentration held constant), no ultrasonic interference was observed. Using an MB^2 solution that strongly attenuated all photoacoustic signal, high powered ultrasound could be used to burst the microbubbles and dramatically enhance photoacoustic contrast (>800-fold increase), providing a new method for spatiotemporal control of photoacoustic signal generation.
 [DOI: 10.1117/1.JBO.19.1.016005]

Keywords: activatable photoacoustic imaging; ultrasound imaging; microbubbles; methylene blue; dual-modality contrast agent.

Paper 130747R received Oct. 16, 2013; revised manuscript received Dec. 4, 2013; accepted for publication Dec. 6, 2013; published online Jan. 6, 2014.

1 Introduction

Photoacoustic (PA) imaging has garnered attention in the last decade because it can make use of optical absorption contrast while providing high ultrasound resolution in deep tissues.[1–3] The principle of PA imaging is that local heat deposition following short laser irradiation pulses generates acoustic waves, and then the propagated waves are detected by conventional ultrasound (US) imaging scanners. PA imaging has been significantly investigated in cancers, brains, hearts, and eyes of small animals.[4–9] Additionally, thanks to the natural fusion of light excitation and US detection, PA imaging systems have been easily merged with existing US imaging systems following minor modifications (e.g., muting of US transmission and collection of raw radio frequency data).[10,11] Because integrated systems have shared acoustic detectors, they present the advantages of conventional US imaging systems, such as portability and real-time imaging capability. At the same time, contrast agents for both imaging modalities have been significantly explored to enhance detection sensitivities and specificities. For example, optically absorbing organic dyes, plasmonic gold nanostructures, and organic nanoparticles have been developed for PA imaging in various biological applications.[12–20] From a clinical point of view, biocompatibility and biodegradability of those nanoparticles for PA imaging have not been meaningfully studied, and thus safety is an ongoing issue as PA moves toward clinical application. So far, clinically approved dyes (i.e., methylene blue and indocyanine green) have the highest chance to be chosen as clinical PA contrast agents.[21,22] Methylene blue is currently being investigated as a PA lymph node tracer in breast cancer.[10,21] For US imaging, microbubbles filled with fluorinated gases are routinely used in clinical practices to map blood flow in hearts, livers, and kidneys.[23] In preclinical studies, microbubbles have been used for US imaging, US-guided drug delivery, and microbubble targeting.[24,25] Dual-functional contrast agents for simultaneous PA and US imaging have recently been reported, such as ink-encapsulated micro- or nanobubbles, encapsulated-gold nanorods human serum albumin shelled microbubbles, and liquid perfluorocarbon nanodroplets with encapsulated plasmonic nanoparticles.[26–28] Recently, we developed microbubbles filled with gases and shelled with porphyrin-lipid conjugates, termed porshe microbubbles.[29] Here, we report a straightforward formulation that gives rise to unique properties, composed of methylene blue microbubbles termed "MB^2," as a dual-modality PA/US contrast agent formed from the simple combination of two clinically used materials. The PA contrast can be derived from the optical absorption of methylene blue followed by laser irradiation, while the US contrast can stem from the acoustic reflection of the transmitted US by gas-filled microbubbles.

[†]These authors equally contributed to this work.

[*]Address all correspondence to: Mansik Jeon, E-mail: msjeon@postech.edu

0091-3286/2014/$25.00 © 2014 SPIE

2 Methods and Materials

2.1 *Synthesis of the Methylene Blue Microbubbles (Referred to as MB^2)*

Unless otherwise noted, chemicals were obtained from Sigma, St. Louis, Missouri. The synthesis process of MB^2 is shown in Fig. 1(a). MB^2 is composed of a lipid shell encapsulating octafluoropropane gas (Concorde Specialty Gases, Eatontown, New Jersey). The following lipids were obtained from Avanti Polar lipids: 1,2-dipalmitoyl-sn-glycero-3-phosphate (DPPA; Avanti # 830855); 1,2-dipalmitoyl-sn-glycero-3-phosphocholine (DPPC; Avanti # 850355); and 1,2-dipalmitoyl-sn-glycero-3-phosphoethanolamine-N-[methoxy(polyethylene glycol)-5000] (MPEG5000; Avanti # 880200). A stock solution of 10 mL of 20 mM methylene blue was made in phosphate-buffered saline (PBS) solution (pH = 7) and diluted to desired concentrations in PBS. DPPA, DPPC, and MPEG5000 stock solutions were made of 20 mg/mL in chloroform and kept at −20°C. Lipid films were made at varying total lipid concentrations while maintaining a molar ratio of DPPC:DPPA:MPEG5000 = 10:1:1.2. Chloroform was used to dissolve the lipids to form a lipid film and solvent was evaporated. The lipids used generated a 1 mg/mL lipid solution unless otherwise noted. The film was a hydrated 750 μL of methylene blue-PBS solution combined with 100 μL of propylene glycol (Bioshop Canada #PRO888.1) and 100 μL of glycerol (Bioshop Canada # GLY001.1) Octafluoropropane gas was added to the vial headspace, the vial was sealed and sonicated to exchange gas within the solution, and then refilled with octafluoropropane. MB^2 was then formed using a vialmix activator (Lantheus Medical Imaging, North Billerica, Massachusetts) for 45 s. As shown in Fig. 1(a), MB^2 synthesis was straightforward and involved hydrating a lipid film with a solution of methylene blue, layering octafluoropropane in the vial, and mechanically agitating the vial to form microbubbles. Photographs of MB^2 and standard microbubbles (hydrated without methylene blue) before and after activation by mechanical agitation are shown in Fig. 1(b).

2.2 *Physical, Optical, and Acoustical Characteristics of MB^2*

After activation, microbubbles were left to sit for 15 min. Microbubbles were gently mixed by hand for 10 s and then decanted for 2 min before extracting a sample from the bottom of the vial. The size distribution and concentration (number of microbubbles/ml) of each formulation was measured with a Coulter Counter Multisizer Z3 (Beckman Coulter Inc., Brea, Canada). Varying volumes of microbubbles were extracted and added to 10 ml of Isoton-II electrolyte solution (Beckman Coulter Inc.) to obtain a microbubble count in the range of 100,000 to 300,000. A background count of buffer was taken prior to measurement and subtracted. Dilution was accounted for in the calculation of the microbubble concentration. The number and size distribution were measured using a 30 μm aperture, which detected microbubbles with diameters in the range of 0.76 to 18 μm. For each microbubble formulation, three samples were measured and averaged. Frequency-dependent attenuation measurements were performed using a narrowband pulse-echo method similar to that used by Goertz et al.[30] Briefly, one transducer (model #595396, 5 MHz, 76 mm focus, 12.7 mm diameter; Olympus NDT Canada Inc., Quebec, Canada) was used to cover a frequency range of 1.5 to 12 MHz sampled in 0.5 MHz increments. Each pulse was generated using an arbitrary waveform generator (Tabor Electronics Ltd., Tel Hanan, Israel) and amplified using a power amplifier (model A-150; ENI, Rochester, NY). The transducer was calibrated for each frequency using a 75-μm needle hydrophone (model 1544; Precision Acoustics, Dorchester, UK) to deliver a peak negative pressure of 25 kPa at the geometric foci, where the face of an aluminum rod serving as a near-perfect reflector was placed. The received echoes were amplified (model AU1579; Miteq, Hauppauge, NY), filtered, and recorded (400 MHz sampling frequency; Agilent Technologies Inc., Palo Alto, CA) for further postprocess analysis. Echoes were recorded prior to and after contrast agent microbubbles were diluted in the gas-equilibriated saline between the transducer and aluminum reflector. Given the ratio of echo amplitudes pre- and postcontrast agent addition and the length in which ultrasound travelled through the bubbly media, the attenuation per unit length could be calculated at each frequency. Optical absorption of the contrast agent was recorded in PBS using the indicated dilution using a spectrophotometer (Lamdba 20, PerkinElmer, Waltham, Massachusetts).

2.3 *Photoacoustic and Ultrasound Imaging of MB^2*

We used two types of combined PA and US imaging systems. The first one was operated with a single-element focused transducer with raster scanning, whereas the other one was modified from a clinical US array system. The system schematic and experimental setup for the first type is shown in Fig. 2(a). The details of the system have been previously reported.[31] Laser pulsing was generated from a tunable laser (Surelite OPO PLUS; Continuum, Santa Clara, California; wavelength tuning range: 650 to 1064 nm) pumped by a Q-switched Nd:YAG laser (SLIII-10; Continuum; 532 nm). The pulse width and repetition rate were 5 ns and 10 Hz, respectively. An optical wavelength of 667 nm (corresponding to the MB^2 peak) was used for PA imaging. Light illuminated the samples via a concave lens, a conical lens, and an

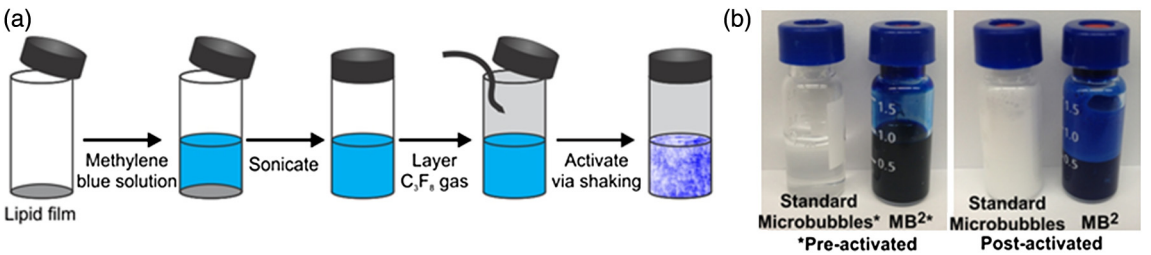

Fig. 1 Synthesis of methylene blue microbubbles (MB^2). (a) Schematic for generating MB^2. (b) Photographs of control microbubbles and MB^2 before and after activation.

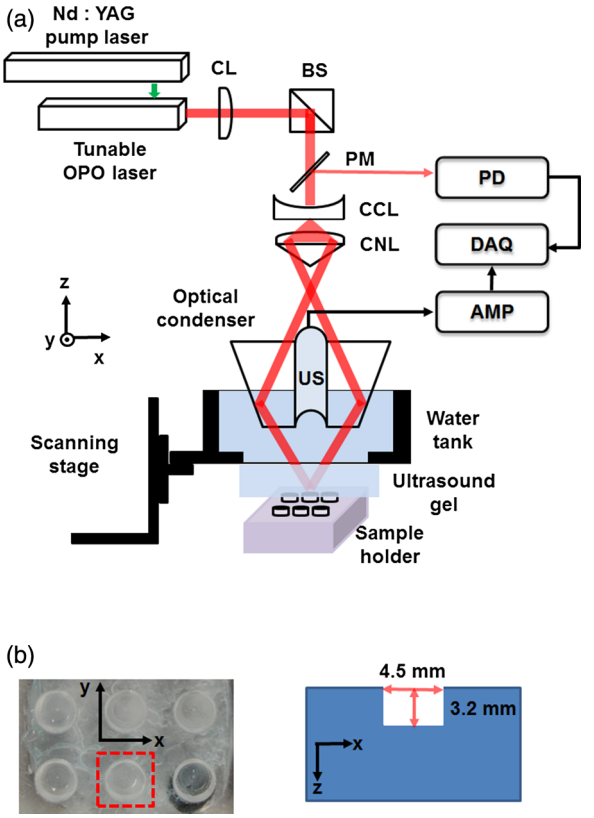

Fig. 2 Experimental setup of a photoacoustic and ultrasound imaging system with a single-element focused transducer and raster scanning. (a) Schematic of the dual modal system. (b) Photograph and dimension of the sample holder. OPO, optical parametric oscillator; PM, partial mirror; CL, collimating lens; BS, beam splitter; CCL, concave lens; CNL, conical lens; US, ultrasound transducer; PD, photo diode; AMP, amplifier; and DAQ, data acquisition.

optical condenser. A home-made water tray was used for acoustic coupling. Induced PA waves were sensed by a single-element acoustic transducer (V308; Olympus NDT, Center Valley, Pennsylvania; 5 MHz center frequency). The PA signals were transferred to a low-noise amplifier (5072PR, Olympus NDT) and were recorded by a data acquisition system. In the US imaging mode, a low-noise amplifier was used as both an ultrasound pulse transmitter and receiver, and the same transducer was used. To form the volumetric data, we used mechanical raster scanning in two transverse directions along the *x*-*y* directions. Figure 2(b) shows the sample holder, which is positioned under the water tank. The sample holder was 4.5 mm in diameter by 3.2 mm in depth filled with aqueous samples. To investigate the restoration of PA signals, we compared the PA and US signals of the MB^2 solution before and after sonication. Further, to confirm this restoration and investigate the clinical applicability of the mechanism, we employed a clinical PA imaging scanner. Figure 3(a) shows a schematic of the combined PA/US imaging system adapted with a clinical US array system (Samsung Medison, Seoul, Korea). 256-channel simultaneous analog-digital converters and external triggering capabilities enabled real-time PA/US imaging. Conventional US and PA images were obtained sequentially and displayed in the US imaging monitor to show both structural US and functional PA (i.e., optical absorption characteristics) images at the same time up to 10 Hz of a PA frame rate. A linear probe with a 7.5 MHz center frequency was used (Samsung Medison, Seoul, Korea). An optical parametric oscillator laser (Phocus HE, Opotek, California) was employed to provide laser pulses with an optical wavelength of 680 nm, a pulse width of 10 ns, and a pulse repetition rate of 10 Hz. A custom-made bifurcated optical fiber bundle was used to deliver light to the sample. For real-time image reconstruction, one-way (receiving mode only) conventional delay-sum beam forming method was employed. One side surface of a rectangular water container was cut opened, and the opened area was covered by a thin transparent window to prevent the leakage of aqueous solutions and enhance acoustic coupling. One optically transparent plastic vial with a diameter of 7 mm was filled with MB^2 (microbubble concentration 0.1 mg/ml; methylene blue concentration, 15 mM), and the other vial was filled with water as a control. Both vials were vertically positioned inside the container, which was filled with water. The PA/US probe was horizontally positioned with its surface directing the center of the vials as shown in Fig. 3(b). Before the microbubbles were destroyed in the solutions, we acquired the control PA image. Then, the US transmission voltage increased to 50 V (the typical voltage, 8 V), US was delivered to the vials for 60 s, and the PA image was again obtained. We repeated this process until the MB^2 was accumulatively exposed to high-voltage US for 10 min.

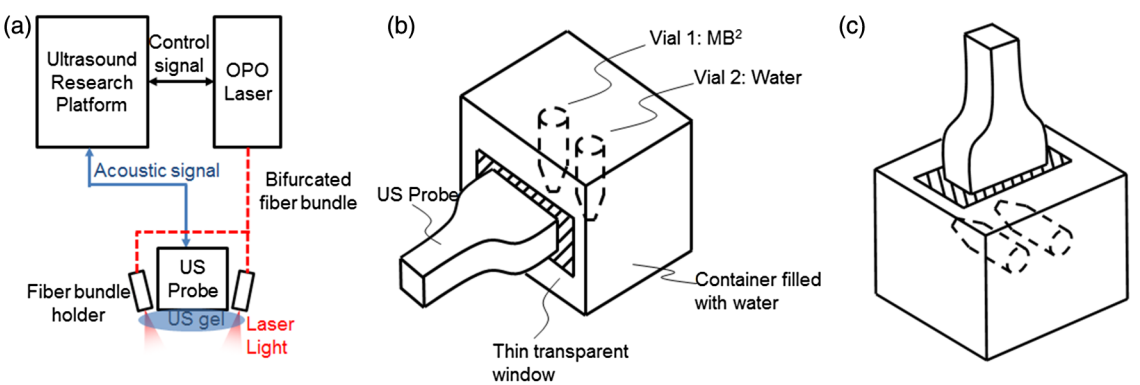

Fig. 3 (a) Schematic of a photoacoustic/ultrasound imaging system adapted with a Samsung Medison US research platform. Experimental setup to pop microbubbles in MB^2 to enhance photoacoustic signals. (b) The vials were positioned vertically, and the ultrasound probe scanned them from the side. (c) The vials were positioned horizontally, and the ultrasound probe scanned them from the top.

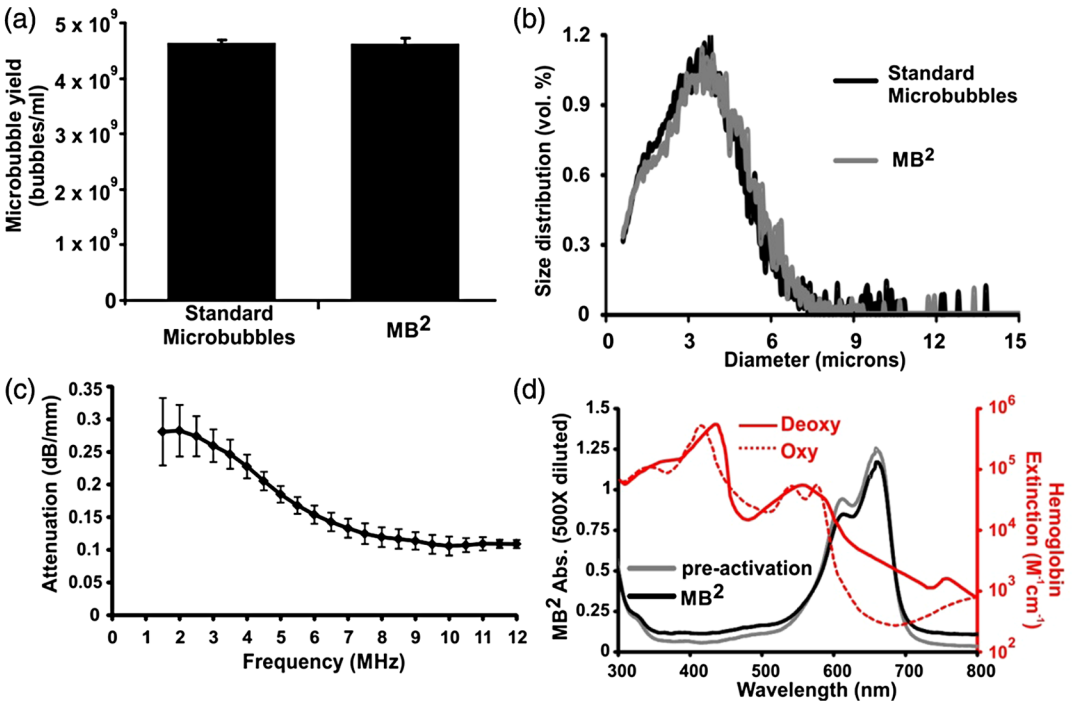

Fig. 4 Physical/optical properties of MB^2. (a) Yields of microbubbles and MB^2. (b) Sizes of control microbubbles and MB^2. (c) Ultrasonic frequency attenuation of MB^2. (d) Optical absorption spectra of MB^2 diluted in phosphate-buffered saline, methylene blue, oxy-hemoglobin, and deoxy-hemoglobin.

3 Results and Discussion

First, we have measured the physical, optical, and mechanical properties of MB^2. Using a highly concentrated solution (15 mM) of methylene blue to hydrate the film had minimal effect on the efficiency of microbubble formation compared to control microbubbles with $\sim 4.5 \times 10^9$ bubbles formed following activation of a 1 mg/mL lipid solution [Fig. 4(a)]. The typical clinical concentration of methylene blue for sentinel lymph node biopsy is ~30 mM. The size of MB^2 was monodispersed with a peak size of just over 3 μm, which was also nearly identical to control microbubbles formed in the absence of methylene blue [Fig. 4(b)]. Due to the similar size distribution of MB^2 to commercial microbubbles, the US attenuation is dominant at the low frequencies (i.e., <6 MHz), which is in agreement with previous attenuation measurements using other lipid-encapsulated agents [Fig. 4(c)].[32,33] The near-infrared absorption generated by MB^2 was intense. Even a 1 in 500 dilution of the MB^2 solution yielded absorption >1 with spectral properties characteristic of methylene blue and thus unaffected by the microbubbles [Fig. 4(d)]. As a comparison, the optical spectra of oxy- and deoxy-hemoglobins are provided.

To investigate the dual-modal imaging capability of MB^2, we photoacoustically and ultrasonically imaged aqueous solutions of MB^2 by varying the concentration of either microbubbles or methylene blue using a single-element US transducer. As shown in Fig. 5(e), the concentration of microbbubles was varied from 0 to 0.25 mg/mL by 0.05 mg/mL increments, while the concentration of methylene blue was fixed at 15 mM. Figures 5(a) and 5(b) show the PA and US images of six samples, respectively. The quantified PA and US signals at various microbubbles concentrations are plotted in Figs. 5(c) and 5(d), respectively. Interestingly, we found a decrease in the PA signals with increasing microbubble concentration. With more than 0.15 mg/mL lipid microbubble concentrations, PA signals were almost identical to the background PA signals. In contrast, ultrasound signals increased as the microbubble concentration mounted and reached a plateau after 0.15 mg/mL lipid when the US signal became saturated. Typically, the amplitude of initial PA pressure can be expressed as $p_0 = \Gamma \eta_{\text{th}} A_e$, where Γ is the Grueneisen parameter (dimensionless); A_e is the specific optical absorption (energy deposition, J/m^3); and η_{th} is the percentage of A_e that is converted into heat. Since the energy deposition (A_e) is equal to the product of the optical absorption coefficient of the target (μ_a) and the optical fluence (F), the PA amplitudes are directly proportional to optical absorption coefficients of the target. In our case, although none of these parameters were modulated, PA signals had interference attenuation. This phenomenon can be explained as follows. As the concentration of the microbubbles increase in the MB^2 solution, the intensity of backscattered US is, certainly, enhanced due to stronger US scattering. However, the initial PA waves are generated inside the medium and start propagating omnidirectionally through the medium. During propagation, the PA waves can be multiply scattered and absorbed (i.e., attenuated) by the surrounding microbubbles. Thus, the measured PA amplitudes decrease with the increase of the microbubbles' concentration in spite of the constant methylene blue concentration. Therefore, by modulating the concentration of microbubbles in the medium, we can attenuate or restore PA signals, which presents a novel mechanism to modulate PA signals.

As shown in Fig. 6(e), the concentration of methylene blue was varied between 0, 1, 5, 10, 15, and 20 mM with the concentration of microbubbles fixed at 0.1 mg/mL. Figures 6(a) and 6(b) show the PA and US images of six samples,

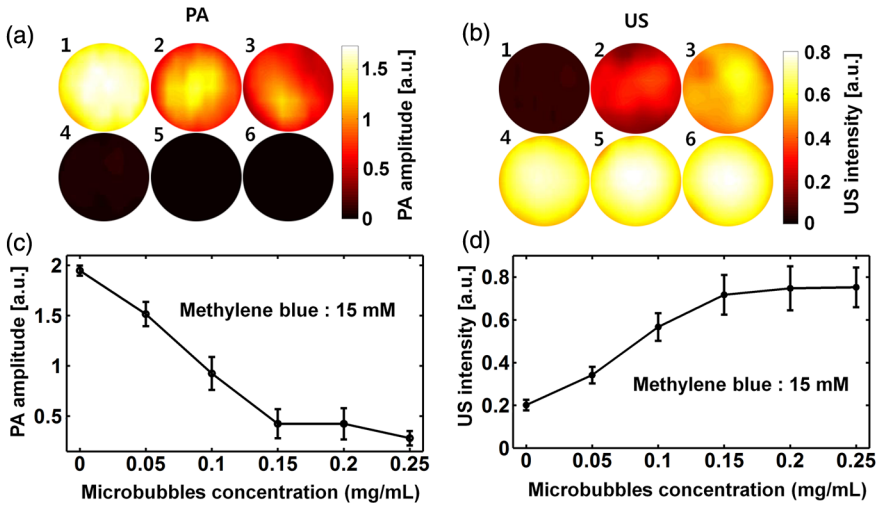

(e)

Microbubbles concentration			
1	0 mg/mL	2	0.05 mg/mL
3	0.1 mg/mL	4	0.15 mg/mL
5	0.2 mg/mL	6	0.25 mg/mL

* Methylene blue concentration, 15 mM

Fig. 5 (a) Photoacoustic and (b) ultrasound imaging of aqueous solutions of MB^2 with various concentrations of microbubbles at a fixed methylene blue concentration (15 mM). (c) Quantified, (a) photoacoustic, and (d) ultrasound signals versus microbubbles concentration. (e) Concentrations of microbubbles and methylene blue in six samples.

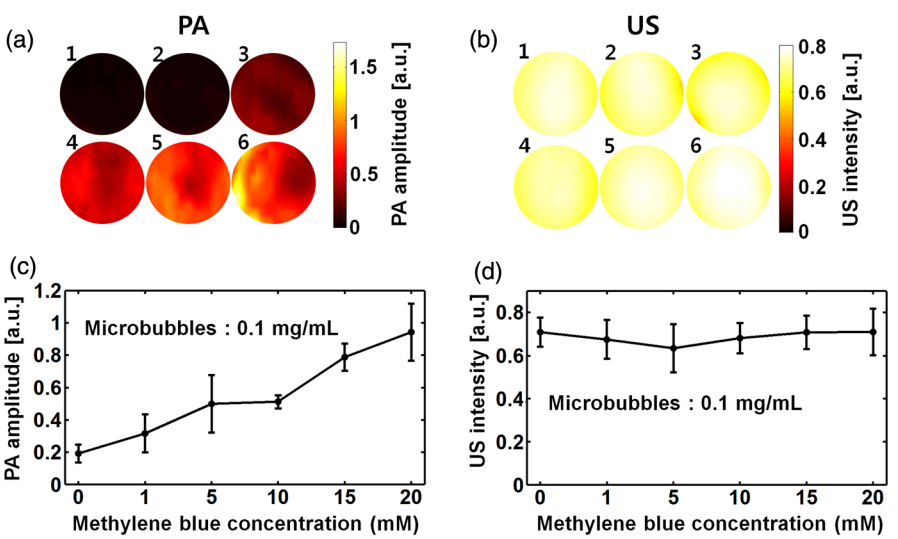

(e)

Methylene blue concentration			
1	0 mM	2	1 mM
3	5 mM	4	10 mM
5	15 mM	6	20 mM

* Microbubbles concentration, 0.1 mg/mL

Fig. 6 (a) Photoacoustic and (b) ultrasound imaging of aqueous solutions of MB^2 with various concentrations of methylene blue at a fixed microbubble concentration (0.1 mg/mL). (c) Quantified, (a) photoacoustic, and (d) ultrasound signals versus methylene blue concentration. (e) Concentrations of methylene blue and microbubbles in six samples.

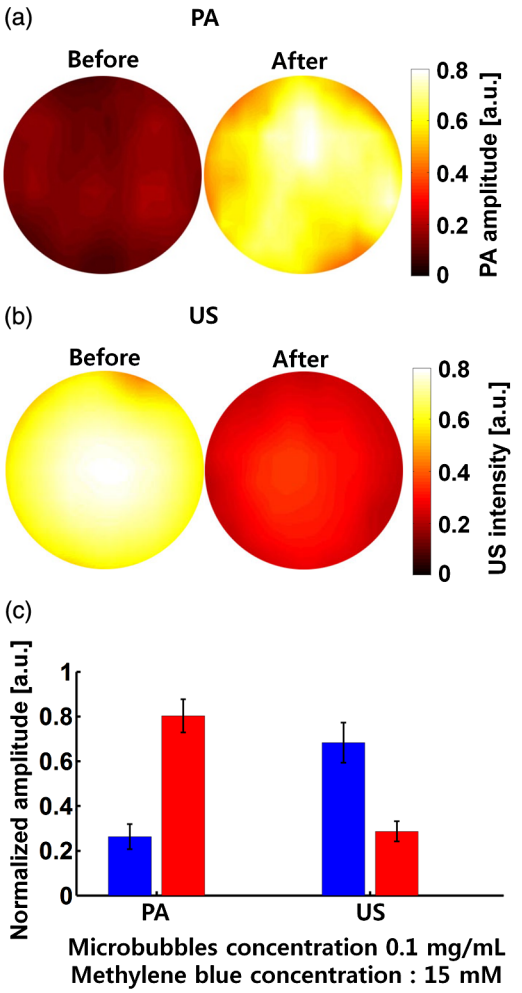

Fig. 7 (a) Photoacoustic and (b) ultrasound imaging of aqueous solutions of MB^2 before and after sonication. (c) Quantified photoacoustic and ultrasound signals before and after sonication.

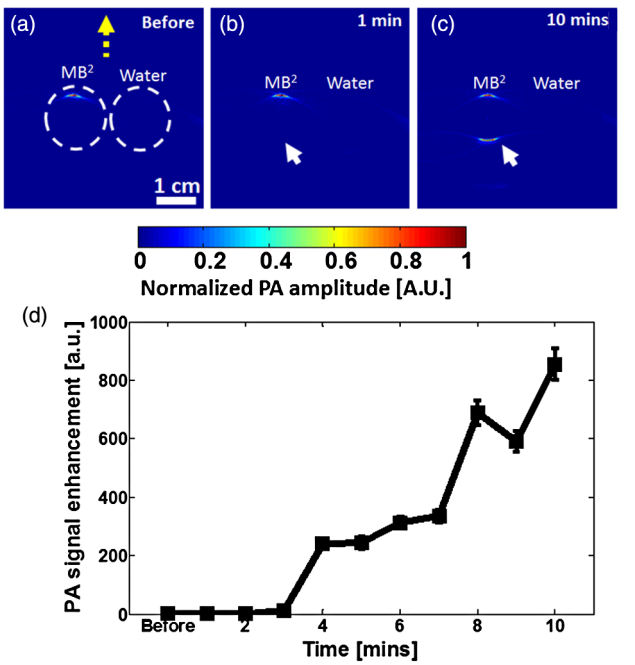

Fig. 8 Photoacoustic images of aqueous solutions of MB^2 before (a) and after 1 min (b) and 10 min (c) of application of high-voltage ultrasound generated by a clinical ultrasound array. (d) Quantified photoacoustic signals versus ultrasound application times. The yellow dotted arrow indicates the position of the ultrasound imaging probe. The white dotted circles indicate the position of two plastic vials filled with MB^2 (left) and water (right). The vials were positioned vertically, and the ultrasound probe scanned them from the side.

respectively. The quantified PA and US signals at various methylene blue concentrations are plotted in Figs. 6(c) and 6(d), respectively. As the concentration of methylene blue increased, consequently the PA signals increased due to greater optical absorption in the solutions. However, the US intensities remained constant because of the fixed bubble concentration. In this case, the PA signals are linearly proportional to the optical absorption coefficient, which is in line with conventional principles of PA wave generation.

To further confirm our findings, we studied the switching of PA and US signals using sonication. We prepared MB^2 with 0.1 mg/mL lipid microbubbles and 15 mM of methylene blue. Then we compared the PA and US signals of the MB^2 solution before and after sonication. Figures 7(a) and 7(b) show the PA and US images of the sample before and after sonication, respectively. The quantified signals are plotted in Fig. 7(c). It is clear that the PA signal was initially attenuated by microbubbles. However, it recovered after the bubbles were destroyed by sonication. The PA amplitude increased 2.5 times. Conversely, the US signals were initially strong, but decreased 2.5 times following sonication.

Moreover, to prove this restoration and explore the practicability of this mechanism, we were able to disrupt the microbubbles in MB^2 and recover the PA signals using a clinically modified PA imaging scanner. As shown in Fig. 8(a), we acquired a control PA image of two vials (e.g., left filled with MB^2 and right filled with water) before the MB^2 was disturbed. The two white dotted circles show the locations of the vials in the medium. The PA probe detected the signals from the top in the image, which was indicated by a yellow dotted arrow [Figs. 3(b) and 8(a)]. The front surface of the left vial (i.e., filled with MB^2) was clearly visible, while the right vial (i.e., filled with water) was photoacoustically invisible. Within 3 min of applying high-voltage US (i.e., 100 Vp-p; corresponding mechanical index, 0.58; the safety limit for diagnostic US, 1.9), we were not capable of recovering PA signals [Fig. 8(b)], but the restoration was significantly enhanced after 10 min [Fig. 8(c)]. Figure 8(d) shows the PA signal enhancement versus high-voltage US application time. The PA signal increased 817 times at 10 min postapplication. Compared with the restoration enhancement obtained using our bench-top system, the improvement using the clinical system was dramatic. We found that the unwanted bulky bubbles in the vial floated up to the top surface over the time period. Thus, when we measured the PA signals from the side [i.e., Fig. 3(b)], our measurements did not have interference from any intact bulky bubbles. However, when we measured the signals from the top (i.e., bench-top experiments), the PA wave propagation was significantly disturbed, which accounts for the only 2.5-fold enhancement observed in our bench-top system. To confirm these findings, we changed the experimental geometry in the clinical system [Fig. 3(c)]. The vials were positioned horizontally, and the US probe scanned them from the top. In this case, the PA signal enhancement was limited to an ~25-fold increase.

4 Conclusions

We successfully developed and showed the utility of MB^2 as a dual-modality contrast agent for US and activatable PA imaging. PA signals were significantly suppressed by the increase of microbubbles in the MB^2 solution (with fixed methylene blue concentration). When methylene blue concentration increased (with fixed microbubble concentration), no change in US intensity was observed. In addition, high powered US generated by a clinical US imaging scanner burst the microbubbles and drastically (817 times) enhanced PA signals, demonstrating a novel approach that can be used to modulate PA signal generation with spatiotemporal control. Conventionally, one or more parameters in the initial PA amplitude (e.g., Grueneisen coefficient, heat conversion efficiency, optical absorption coefficient, or optical fluence) within an object should be adjusted to control the PA signals. However, none of these parameters were involved in our approach. In terms of a molecular imaging perspective, both PA and US imaging typically suffer from strong background signals. To improve signal-to-noise ratios and clearly delineate the agent distribution, the background signals should be significantly suppressed, which can be easily done by switching between PA and US signals. Therefore, the dual-modality PA/US imaging system with a combination of the dual-modality agent, MB^2, can be applied to image cancers, monitor drug delivery, and visualize internal organs such as bladders and lymph nodes. From a clinical point of view, both methylene blue and microbubbles have been widely used in clinical practices. From an imaging system perspective, both custom-made bench-top and clinically feasible imaging scanners have been utilized in this study. Thus, there are few barriers impeding the clinical translation of MB^2 using clinical PA imaging systems.

Acknowledgments

This work was supported by the research fund from Samsung Medison to C.K. and J.L., and NRF grant of Korea government [Ministry of Science, ICT and Future Planning (MSIP)] (2011-0030075), and MSIP, Korea, under the IT Consilience Creative Program (NIPA-2013-H0203-13-1001) supervised by the National IT Industry Promotion Agency to C.K.

References

1. P. Beard, "Biomedical photoacoustic imaging," *Interface Focus* **1**(4), 602–631 (2011).
2. C. Kim, C. Favazza, and L. H. V. Wang, "In vivo photoacoustic tomography of chemicals: high-resolution functional and molecular optical imaging at new depths," *Chem. Rev.* **110**(5), 2756–2782 (2010).
3. L. H. V. Wang and S. Hu, "Photoacoustic tomography: in vivo imaging from organelles to organs," *Science* **335**(6075), 1458–1462 (2012).
4. J. Laufer et al., "In vivo preclinical photoacoustic imaging of tumor vasculature development and therapy," *J. Biomed. Opt.* **17**(5), 056016 (2012).
5. J. J. Yao, K. I. Maslov, and L. H. V. Wang, "In vivo photoacoustic tomography of total blood flow and potential imaging of cancer angiogenesis and hypermetabolism," *Technol. Cancer Res. Treat.* **11**(4), 301–307 (2012).
6. J. J. Yao et al., "Noninvasive photoacoustic computed tomography of mouse brain metabolism in vivo," *Neuroimage* **1**(64), 257–266 (2013).
7. J. Laufer et al., "In vivo photoacoustic imaging of mouse embryos," *J. Biomed. Opt.* **17**(6), 061220 (2012).
8. R. J. Zemp et al., "Realtime photoacoustic microscopy of murine cardiovascular dynamics," *Opt. Express* **16**(22), 18551–18556 (2008).
9. S. L. Jiao et al., "Photoacoustic ophthalmoscopy for in vivo retinal imaging," *Opt. Express* **18**(4), 3967–3972 (2010).
10. C. Kim et al., "Performance benchmarks of an array-based hand-held photoacoustic probe adapted from a clinical ultrasound system for non-invasive sentinel lymph node imaging," *Philos. Trans. R. Soc. A* **369** (1955), 4644–4650 (2011).
11. S. A. Ermilov et al., "Laser optoacoustic imaging system for detection of breast cancer," *J. Biomed. Opt.* **14**(2), 024007 (2009).
12. C. Kim et al., "Sentinel lymph nodes and lymphatic vessels: noninvasive dual-modality in vivo mapping by using indocyanine green in rats-volumetric spectroscopic photoacoustic imaging and planar fluorescence imaging," *Radiology* **255**(2), 442–450 (2010).
13. B. Wang et al., "Photoacoustic tomography and fluorescence molecular tomography: a comparative study based on indocyanine green," *Med. Phys.* **39**(5), 2512–2517 (2012).
14. E. Morgounova et al., "Photoacoustic lifetime contrast between methylene blue monomers and self-quenched dimers as a model for dual-labeled activatable probes," *J. Biomed. Opt.* **18**(5), 056004 (2013).
15. X. Cai et al., "In vivo quantitative evaluation of the transport kinetics of gold nanocages in a lymphatic system by noninvasive photoacoustic tomography," *ACS Nano* **5**(12), 9658–9667 (2011).
16. C. Kim et al., "In vivo photoacoustic mapping of lymphatic systems with plasmon-resonant nanostars," *J. Mater. Chem.* **21**(9), 2841–2844 (2011).
17. J. V. Jokerst et al., "Gold nanorods for ovarian cancer detection with photoacoustic imaging and resection guidance via Raman imaging in living mice," *ACS Nano* **6**(11), 10366–10377 (2012).
18. T. Z. H. Qin et al., "Gadolinium(III)-gold nanorods for MRI and photoacoustic imaging dual-modality detection of macrophages in atherosclerotic inflammation," *Nanomedicine* **8**(10), 1611–1624 (2013).
19. J. F. Lovell et al., "Porphysome nanovesicles generated by porphyrin bilayers for use as multimodal biophotonic contrast agents," *Nat. Mater.* **10**(4), 324–332 (2011).
20. Z. B. Zha et al., "Biocompatible polypyrrole nanoparticles as a novel organic photoacoustic contrast agent for deep tissue imaging," *Nanoscale* **5**(10), 4462–4467 (2013).
21. C. Kim et al., "Deeply penetrating in vivo photoacoustic imaging using a clinical ultrasound array system," *Biomed. Opt. Express* **1**(1), 278–284 (2010).
22. C. Kim et al., "Handheld array-based photoacoustic probe for guiding needle biopsy of sentinel lymph nodes," *J. Biomed. Opt.* **15** (4), 046010 (2010).
23. S. R. Wilson and P. N. Burns, "Microbubble-enhanced US in body imaging: what role?," *Radiology* **257**(1), 24–39 (2010).
24. G. M. Lanza and S. A. Wickline, "Targeted ultrasonic contrast agents for molecular imaging and therapy," *Curr. Prob. Cardiol.* **28**(12), 625–653 (2003).
25. J. Song et al., "Stimulation of arteriogenesis in skeletal muscle by microbubble destruction with ultrasound," *Circulation* **106**(12), 1550–1555 (2002).
26. C. Kim et al., "Multifunctional microbubbles and nanobubbles for photoacoustic and ultrasound imaging," *J. Biomed. Opt.* **15**(1), 010510 (2010).
27. Y. H. Wang et al., "Photoacoustic/ultrasound dual-modality contrast agent and its application to thermotherapy," *J. Biomed. Opt.* **17**(4), 045001 (2012).
28. K. Wilson, K. Homan, and S. Emelianov, "Biomedical photoacoustics beyond thermal expansion using triggered nanodroplet vaporization for contrast-enhanced imaging," *Nat. Commun.* **3**(618), 1–10 (2012).
29. E. Huynh et al., "Porphyrin shell microbubbles with intrinsic ultrasound and photoacoustic properties," *J. Am. Chem. Soc.* **134**(40), 16464–16467 (2012).
30. D. E. Goertz, N. de Jong, and A. F. W. van der Steen, "Attenuation and size distribution measurements of definity (TM) and manipulated definity (TM) populations," *Ultrasound Med. Biol.* **33**(9), 1376–1388 (2007).
31. C. Kim, M. Jeon, and L. V. Wang, "Nonionizing photoacoustic cystography in vivo," *Opt. Lett.* **36**(18), 3599–3601 (2011).
32. J. M. Gorce, M. Arditi, and M. Schneider, "Influence of bubble size distribution on the echogenicity of ultrasound contrast agents—a study of SonoVue (TM)," *Invest. Radiol.* **35**(11), 661–671 (2000).
33. K. Sarkar et al., "Characterization of ultrasound contrast microbubbles using in vitro experiments and viscous and viscoelastic interface models for encapsulation," *J. Acoust. Soc. Am.* **118**(1), 539–550 (2005).

Mansik Jeon is currently a research associate of Future IT Innovation Laboratory at Pohang University of Science and Technology. He received the PhD degree in electrical engineering from Kyungpook National University, Daegu, South Korea in 2011. His research interests are developing novel optical imaging systems including photoacoustic tomography, optical coherence tomography, and their handheld probes.

Chulhong Kim is currently an assistant professor of creative IT engineering at Pohang University of Science and Technology. He studied for his PhD degree at Washington University in St. Louis, St. Louis, Missouri, under the supervision of Dr. Lihong Wang, Gene K. Beare distinguished professor. His research interests are in the development of nonionizing and noninvasive novel biomedical imaging techniques, including photoacoustic tomography, ultrasound-modulated optical tomography, fluorescence imaging, laser speckle contrast imaging, and ultrasonic imaging.

Biographies of the other authors are not available.